Comparative Analysis of ADRC & PI Controllers Used in Wind Turbine System Driving a DFIG

Mohammed ARBAOUI*, Ahmed ESSADKI*, Tamou NASSER**, Haitam CHALAWANE***

* Electrical Engineering Department of ENSET Rabat, Mohammed V University, Morocco

** Communication Networks Department of ENSIAS Rabat, Mohammed V University, Morocco

*** Electrical Engineering Department of ENSET Rabat, Mohammed V University, Morocco

(mohammed.arbaoui@um5s.net.ma, ahmed.essadki1@gmail.com, tnasser@ensias.ma, haitam_chalawane@um5.ac.ma)

‡ Corresponding Author; Mohammed ARBAOUI, Morocco, Tel: +212 624 391 556,
mohammed.arbaoui@um5s.net.ma

Received: 04.04.2017 Accepted:26.04.2017

Abstract- As part of this work, we study the modelling and control strategies of the variable speed wind turbine based on DFIG, which remains the configuration most adopted and the most installed in the wind farms in the world. The MPPT algorithm without speed control is used to extract the maximum of the power converted by the turbine in case of weak winds. To control the active and reactive powers generated by the DFIG in an independent manner, vector control with stator flux orientation is established using two approaches: Conventional control by PI regulators synthesized using the internal model control is presented in first place, and then followed by the proposed robust control based on the Active Disturbance Rejection Control (ADRC). The performances of the two control strategies in question were compared to prove the effectiveness of the proposed control. Encouraging simulation results have been obtained using Matlab/Simulink Software.

Keywords ADRC, modeling, DFIG, ESO, wind energy, MPPT.

1. Introduction

The constant growth of energy consumption in all its forms, and the associated polluting effects, mainly caused by the burning of fossil fuels, are at the heart of the issue of sustainable development and environmental care. Faced with these problems, the world is massively turned to forms of energy called "renewable" that offer the ability to generate electricity cleanly and above all, to a lesser resource dependence, among these, we find wind power that represents a significant potential and provide sustainable energy source [1, 2, 3].

Worldwide, wind energy has grown strongly, leading researchers in electrical engineering to carry out investigations in order to increase the efficiency of electromechanical conversion on the one hand and to improve the quality of the electrical energy provided on the other hand [4].

Due to the limitations presented by the PI regulator, and to improve the control of the wind chain a new robust control based on the active rejection of disturbances has been adopted.

The modelling of the various constituents of the wind system have been presented, such as the model of turbine, transmission shaft, and the doubly fed induction generator, As well as establishing the MPPT control strategy without speed control, which not require an additional anemometer for measurement [5].

Vector control has been established using PI, and the control method based on active disturbance rejection to ensure an independent control of the active and reactive powers of the DFIG, in the end we conclude by a robustness test comparison between the two command strategies, showing the effectiveness of the ADRC.

2. System Modelling

This part presents a detailed modelling of wind turbine system.

2.1. Turbine model

Consider a wind turbine equipped with blades of length R driving a generator through a gain speed multiplier G represented in Fig.1, where Ω_t, Ω_m represent the turbine speed and the mechanical speed of the DFIG:

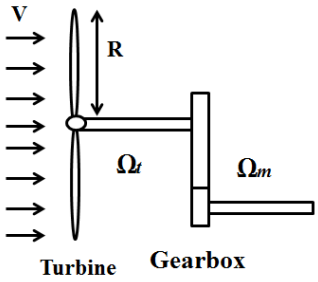

Fig. 1. Wind turbine

The wind speed v, applied to the wind blades, causes its rotation and creates a mechanical power on turbine shaft denoted P_{aero} and expressed by Eq. (1). Where λ represent the speed ratio, β is the angle of the pitch, equal to 0 in this paper, ρ is the air density, generally taken equal to 1.225kg / m3:

$$P_{aero} = C_P(\lambda,\beta)P_v = C_P(\lambda,\beta)\frac{\rho s v^3}{2} \quad (1)$$

The turbine converts the wind's aerodynamic energy into mechanical energy. Its aerodynamic torque T_{aero} is given by the following expression:

$$T_{aero} = \frac{1}{2.\Omega_t} C_P(\lambda,\beta)\rho s v^3 \quad (2)$$

According to Betz limit the maximum wind power can be extracted by wind turbine is 59%, in real case the aerodynamic efficiency is about 48% [6]. This percentage is usually known as the power facto rC_P, which depends on the characteristics of the turbine (the speed ratio and the pitch angle):

$$C_P(\lambda,\beta)) = 0.5176\left(\frac{116}{\lambda'} - 0.4\beta - 5\right)e^{\frac{-21}{\lambda'}} + 0.0068\lambda \quad (3)$$

$$\lambda = \frac{\Omega_t.R}{V} \quad (4)$$

$$\frac{1}{\lambda'} = \frac{1}{\lambda + 0.08\beta} - \frac{0.035}{\beta^3 + 1} \quad (5)$$

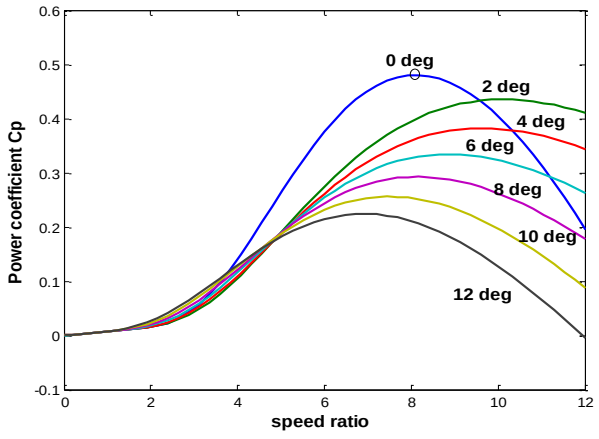

Fig. 2. Power coefficient characteristics for various values of pitch angle β

2.2. Gearbox and mechanical model

The mechanical part of the turbine comprises three blades of length R, they are fixed on a drive shaft rotating at a speed Ωt, connected to a gain multiplier G. This multiplier drives the electric generator.

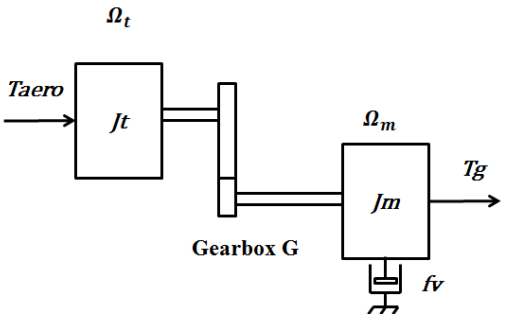

Fig. 3. Mechanical model of wind turbine

$$T_g = \frac{Taero}{G} \quad (6)$$

$$\Omega_t = \frac{\Omega_m}{G} \quad (7)$$

$$J = \frac{J_t}{G^2} + J_m \quad (8)$$

$$T_{mec} = T_g - T_{em} - T_{vis} \quad (9)$$

$$J\frac{d\Omega_m}{dt} = T_{mec} \quad (10)$$

Where $(T_g, T_{em}, T_{vis}, T_{mec})$ are respectively multiplier torque, electromagnetic torque, viscous friction torque $f\Omega_m$, and the mechanical torque.

The Fig (4) represents the schematic model of the turbine:

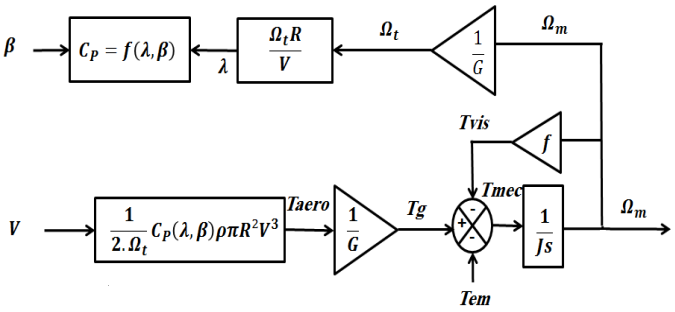

Fig. 4. Schematic Model of the entire wind turbine

2.3. The MPPT control strategy

The wind turbines used for the electricity production must recuperate the maximum energy available in the wind by acting on the mechanical or electrical part.

The control device for this situation must force a reference torque to permit the DFIG to turn at a flexible speed to guarantee an ideal operating point to maximize the use of the wind turbine [7].

The speed ratio in this specific circumstance should be kept at its optimal value over a specific wind speed in order to set C_P to its maximum value [5].

That way we can get the reference torque T_{em_ref} from the Eq. (11) to allow the DFIG to turn at variable speed to reach the optimum operating permanently.

$$T_{em\_ref} = \frac{1}{2\lambda_{opt}^3} Cp_{max}\rho\pi R^5\hat{\Omega}^2 \quad (11)$$

The measurement of wind speed is difficult, an estimate of its value can be obtained [8, 9].

$$v = \frac{R\tilde{\Omega}_t}{\lambda_{opt}} \tag{12}$$

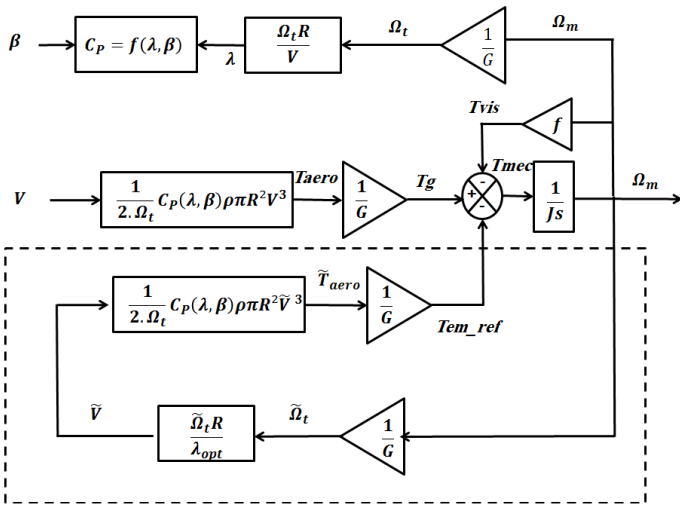

Fig. 5. Block diagram of the maximization of the extracted power

2.4. DFIG modelling

The doubly fed induction generator driven by wind turbine is the most interesting generator because of its intrinsic characteristics, such as variable speed operation, a low level of mechanical stress, and small power converters due to the limitation of the power circulating in the rotor circuit |g.Ps| (30% of the nominal power of the machine), it also helps increasing total system efficiency [10, 11].

The wind energy conversion chain based on the double fed induction machine connected directly to the network by its stator and through back-to-back converter (rotor-side and grid-side) by its rotor [12].

The active and reactive power of this type of generator can be controlled independently by acting on the rotor side converter RSC [13].

The modelling of DFIG in the park reference will be discussed in this section in order to get out the key equations to control the machine.

The subscripts s, r, d, q, m indicate respectively stator, rotor, direct, quadrature, and mutual.

The classical electrical equations:

$$\begin{cases} V_{sd} = R_s i_{sd} + \frac{d\phi_{sd}}{dt} - \omega_s \phi_{sq} \\ V_{sq} = R_s i_{sq} + \frac{d\phi_{sq}}{dt} + \omega_s \phi_{sd} \\ V_{rd} = R_r i_{rd} + \frac{d\phi_{rd}}{dt} - \omega_r \phi_{rq} \\ V_{rq} = R_r i_{rq} + \frac{d\phi_{rq}}{dt} + \omega_r \phi_{rd} \end{cases} \tag{13}$$

The flux equations are given as follows, where L is the inductance:

$$\begin{cases} \phi_{sd} = L_s i_{sd} + L_m i_{rd} \\ \phi_{sq} = L_s i_{sq} + L_m i_{rq} \\ \phi_{rd} = L_r i_{rd} + L_m i_{sd} \\ \phi_{rq} = L_r i_{rq} + L_m i_{sq} \end{cases} \tag{14}$$

Electromagnetic torque Tem can be expressed in Eq. (15), p represents the poles number:

$$T_{em} = \frac{3}{2} p \frac{L_m}{L_s} (\phi_{sq} i_{rd} - \phi_{sd} i_{rq}) \tag{15}$$

The active and reactive powers in the stator and rotor of the DFIG are given respectively:

$$\begin{cases} P_S = V_{sd} i_{sd} + V_{sq} i_{sq} \\ Q_S = V_{sq} i_{sd} - V_{sd} i_{sq} \\ P_r = V_{rd} i_{rd} + V_{rq} i_{rq} \\ Q_r = V_{rq} i_{rd} - V_{rd} i_{rq} \end{cases} \tag{16}$$

2.5. DFIG model with stator flux orientation

To ensure an independent control of active and reactive power [14], the modelling of the machine is established in a two-phase d-q reference system so as to highlight the relations between the stator and rotor [15], by adopting a constant stator flux oriented on d axis and the hypothesis of a negligible stator resistance Rs (for medium and high power machines used in wind turbines) as shown in Fig.6, we get ($\phi_{sd} = \phi_s$, $\phi_{sq} = \frac{d\phi_{sq}}{dt} = 0$, $V_{sd} = 0$ and $V_{sq} = V_s = \omega_s \phi_{sd}$)

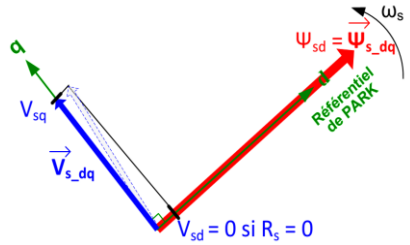

Fig. 6. Orientation of the stator flux

So under this assumption, the rotor voltages to impose to the DFIG can be expressed by:

$$\begin{cases} V_{rd} = R_r i_{rd} + L_r \sigma \frac{di_{rd}}{dt} - g\omega_s L_r \sigma i_{rq} \\ V_{rq} = R_r i_{rq} + L_r \sigma \frac{di_{rq}}{dt} - g\omega_s L_r \sigma i_{rd} + g\omega_s \frac{V_s L_m}{L_s \omega_s} \end{cases} \tag{17}$$

Where $\sigma = (1 - \frac{L_m^2}{L_r L_s})$ is the dispersion coefficient.

From the Eq. (16) we have:

$$\begin{cases} P_S = -\frac{V_s L_m}{L_s} i_{rq} \\ Q_S = \frac{V_s \phi_s}{L_s} - \frac{V_s L_m}{L_s} i_{rd} \end{cases} \tag{18}$$

Finally, the electromagnetic torque becomes:

$$T_{em} = -\frac{3}{2} p \frac{L_m}{L_s} \phi_s i_{rq} \tag{19}$$

From Eq. (18) we can deduce that the active power is controlled by acting on the quadrature component of the rotor current of the DFIG irq, the direct component ird is used to control the reactive power [16], as exposed in Fig.7:

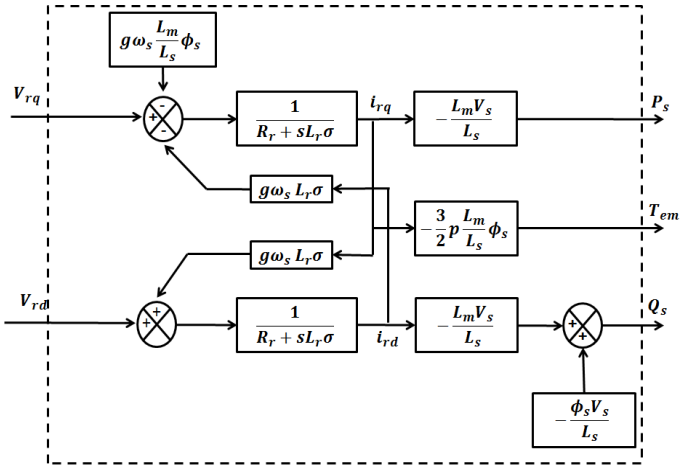

Fig. 7. The internal model of the DFIG

3. Controllers Synthesis

This part is devoted to the synthesis of the control strategies:

3.1 PI controller synthesis

To ensure that the active and reactive powers of the DFIG follow their references, a PI regulator Eq. (20) is essential.

The corrected closed loop system is shown in Fig.8.

$$R(s) = K_p + \frac{K_i}{s} \tag{20}$$

Where:

- K_p: is the proportional gain controller.
- K_i: is the integral controller gain

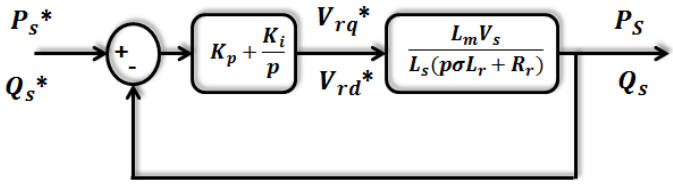

Fig. 8. Structure of PI controller

$$\begin{cases} K_p = K_i \sigma T_r = \frac{\sigma L_s L_r}{\tau L_m V_s} \\ K_i = \frac{L_s R_r}{\tau L_m V_s} \end{cases} \tag{21}$$

τ is the time constant of our system, which is taken equal to 1 ms.

3.2 Active Disturbance Rejection Control controller design

The analysis and synthesis of a control law for dynamic systems has long been the subject of many research.

The study of stability, rejection of perturbation, reference tracking, of these systems often requires full or partial knowledge of the model of the process to be controlled. This imposes knowledge of its behavior, the evolution of its components over time, its interactions with the external environment and the constraints it undergoes.

While the systems vary in time, uncertain (variation of the internal parameters of the physical plant) and are non-linear, the conventional regulators like PID or PI regain their performances in high degradation due to different perturbations that influence the model used initially for their design.

As a result of these disadvantages, a method founded by Han in 1995, known as the Active Disturbance Rejection Control (ADRC), based on the ESO or extended state observer that constitutes its core that estimate and cancel the various external (as voltage dip…) and internal (modelling uncertainties) disturbances of the system in real time using control signal [8].

Consider a first order system where y represents the output signal and u the input signal:

$$\begin{aligned} \dot{y} &= f_1(y, d, t) + bu \\ &= f_1(y, d, t) + (bu - b_0 u) + b_0 u \\ &= f(y, d, t) + b_0 u \end{aligned} \tag{22}$$

Here $f(y, d, t)$ or f, represents the total disturbance which associated internal and external disturbances, d is the external disturbance, b0 is a known parameter.

The Eq. (23) describes the state space of the system:

$$\begin{cases} \dot{x}_1 = x_2 + b_0 u \\ \dot{x}_n = h \\ y = x_1 \\ \dot{f} = h \end{cases} \tag{23}$$

We put $h = \dot{f}$.

The ADRC relies on the proper functioning of the ESO extended state observer and its ability to make a good estimate of disturbances [17]. A dynamic observer has the following form:

$$\begin{cases} \dot{\hat{x}}_1 = \hat{x}_2 + l_1(y - \hat{x}_1) + b_0 u \\ \dot{\hat{x}}_2 = l_2(y - \hat{x}_1) \end{cases} \tag{24}$$

Where $\hat{x} = [\hat{x}_1, \hat{x}_2]^T$, and l_i, i=1,2 is the chosen observer gain vector.

The determination of the matrix L will allow fixing arbitrarily the poles of the observer at $-\omega_0$ "bandwidth parameterization", and to choose the eigenvalues of the matrix (A-LC) so that it is Hurwitz [18, 19]. Consider the characteristic equation:

$$\begin{aligned} \lambda_0(s) &= \det(sI - (A - LC)) = s^2 + l_1 s + l_2 \\ &= s^2 + \omega_0 \alpha_1 s + {\omega_0}^2 \alpha_2 = (s + \omega_0)^2 \end{aligned} \tag{25}$$

Where $[l_1, l_2] = [\omega_0 \alpha_1, {\omega_0}^2 \alpha_2]$, ω_0 represent the observer bandwidth which can be determined using pole placement technique, $\alpha_i = \frac{(n+1)!}{i!(n+1-i)!}$; i=1,2.

The estimated variables $\hat{x}_1(t) \to \hat{y}(t)$ and $\hat{x}_2(t) \to \hat{f}(t)$ are used to actively eliminate the perturbation f by the application of command signal u:

$$u = \frac{u_0 - \hat{f}}{b_0} \tag{26}$$

So our system is reduced to a simple integrator easily controlled via a proportional correction K_p as described in Eq. (28).

Where, r represents the reference signal to follow.

$$\dot{y} = f + b_0 \frac{u_0 - \hat{f}}{b_0} = f - \hat{f} + u_0 \approx u_0 = K_p(r - \hat{y}) \quad (27)$$

$$u_0 = K_p(r - \hat{y}) \quad (28)$$

In practice ω_0 is often chosen in a range of ω_0=3~ 7ω_c with $\omega_c = K_p$ is the closed loop desired [8].

The combination of the linear ESO and the corrector represents the linear ADRC.

The ADRC structure is given in Fig.9:

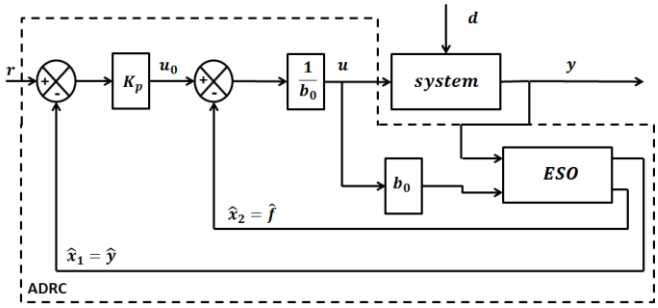

Fig. 9. Structure of the linear ADRC first order

4. Decoupled Control Strategy of Active and Reactive Power

The main control objective of the RSC (rotor side converter) is to control in an independent manner the active and reactive powers. This control consists of three stages: Power control, current control and converter control as shown in Fig. 10:

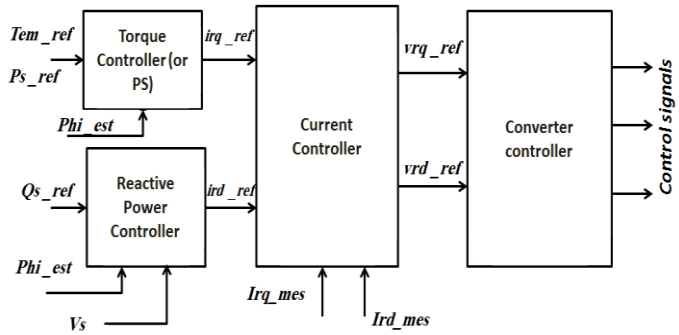

Fig. 10. Structure of RSC [17]

The control of the DFIG via rotor side converter must ensure the necessary torque to extract the maximum power.

The active and reactive powers being controlled by the quadrature i_{rq} and the direct component i_{rd} respectively according to the equation 18:

The expression of the rotor current i_{rq} can be deduced from the active power equation mentioned in Eq. (18):

$$i_{rq\_ref} = -\frac{L_s}{V_s L_m} P_{S\_ref} \quad (29)$$

Similarly, it is possible to express the current i_{rd} that is used to control the reactive power Q_S from Eq. (18) by:

$$i_{rd\_ref} = \frac{\phi_s}{L_m} - \frac{L_s}{L_m V_s} Q_{s\_ref} \quad (30)$$

4.1 Power control using the conventional PI controller

The reference rotor voltages are evaluated from the Eq. (17), and the coupling terms are estimated by measuring the stator and rotor currents and the pulsation of the rotor currents ω_r as Follows [20]:

$$\begin{cases} \tilde{e}_d = L_r \omega_r \sigma \hat{i}_{rd} \\ \tilde{e}_q = L_r \omega_r \sigma \hat{i}_{rq} \end{cases} \quad (31)$$

Figure 11 shows the indirect power control scheme that uses a PI controller:

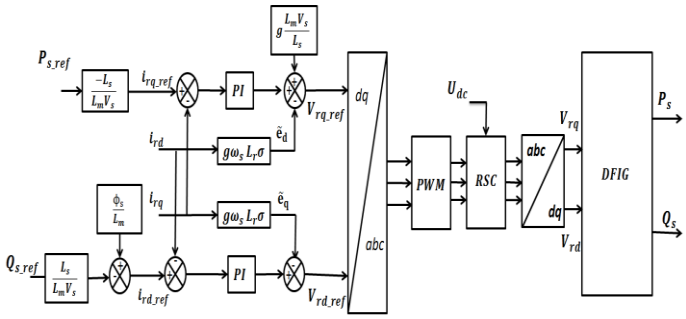

Fig. 11. Scheme of indirect power control (IPC) using PI

4.2 Power control by ADRC

This time the ADRC strategy is used to control the rotor currents as shown in Fig. 12, by imposing reference rotor voltages to the RSC converter that generates the control commands using the Pulse Width Modulation (PWM).

The rotor currents are rearranged to be written in the form:

$$\begin{cases} \frac{di_{rd}}{dt} = -\frac{R_r}{\sigma L_r} i_{rd} + g\omega_s i_{rq} + \frac{1}{\sigma L_r} V_{rd} \\ \frac{di_{rq}}{dt} = -\frac{R_r}{\sigma L_r} i_{rq} - g\omega_s i_{rd} - g\omega_s \frac{L_m}{\sigma L_r L_s} \phi_s + \frac{1}{\sigma L_r} V_{rq} \end{cases} \quad (32)$$

We put these expressions in the form:

$$\frac{di_{rd}}{dt} = f_d(i_{rd}, d, t) + b_0 u(t)$$

Where:

$$\begin{cases} f_d = -\frac{R_r}{\sigma L_r} i_{rd} + g\omega_s i_{rq} + (\frac{1}{\sigma L_r} - b_0) V_{rd} \\ u = V_{rd} \qquad b_0 = \frac{1}{\sigma L_r} \end{cases} \quad (33)$$

$$\frac{di_{rq}}{dt} = f_q(i_{rq}, d, t) + b_0 u(t)$$

Where:

$$\begin{cases} f_q = -\frac{R_r}{\sigma L_r} i_{rq} - g\omega_s i_{rd} - g\omega_s \frac{L_m}{\sigma L_r L_s} \phi_s + (\frac{1}{\sigma L_r} - b_0) V_{rq} \\ u = V_{rq} \qquad b_0 = \frac{1}{\sigma L_r} \end{cases} \quad (34)$$

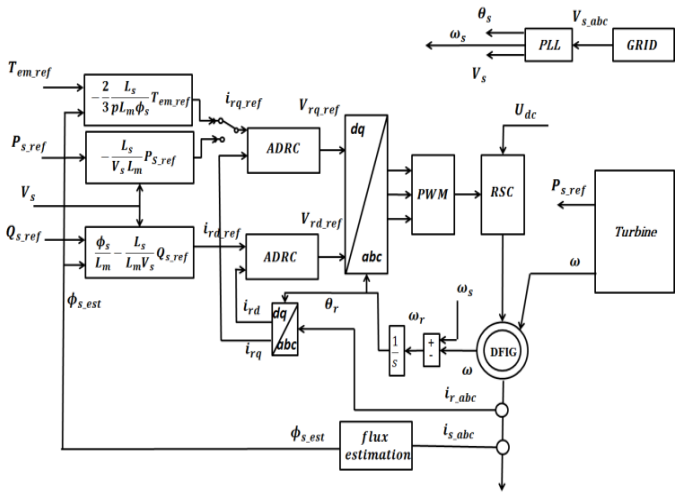

Fig. 12. IPC using ADRC controller

5. Results of the Simulation

5.1 Results obtained

The control results of the wind system are presented and discussed in this section, the parameters are given in Appendix.

Figure 13 shows the mechanical speed of the DFIG, it is necessary to maintain the slip value g (± 30%) for a stable operation of the DFIG reason.

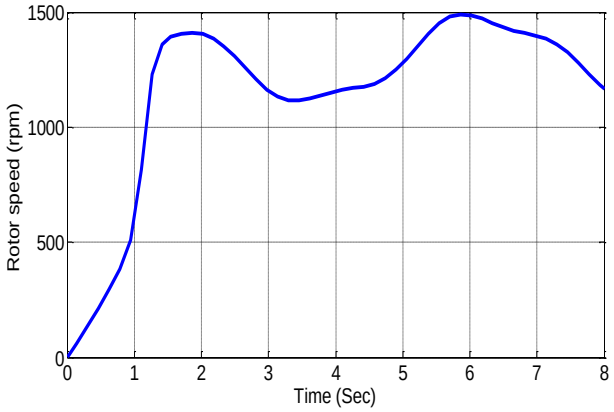

Fig. 13. Mechanical Rotor Speed

From Fig.13-14-15 show that the increase in wind speed implies an increase in the speed of the turbine, however this increase, the power coefficient Cp and the speed ratio λ maintained at their optimal values (C_{pmax} = 0.48, λ_{opt} = 8.1) even if the small decreases sometimes, which shows the effectiveness of the MPPT control.

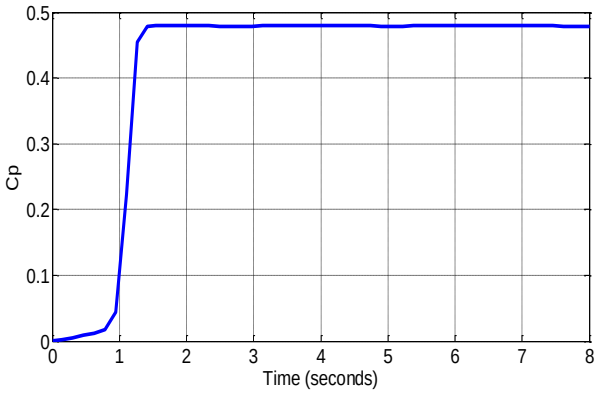

Fig. 14. Power coefficient Cp

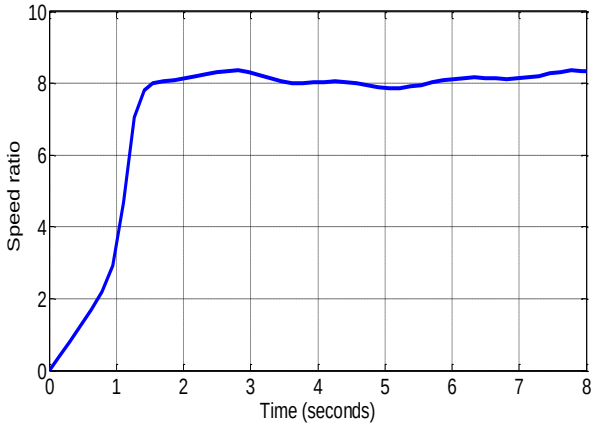

Fig. 15. Speed ratio λ

The reference reactive power varies in the following form over time:

$$\begin{cases} 0 \le t \le 3 \;\Rightarrow\; Q_{s_{ref}} = 0 \text{ VAR} \\ 3 \le t \le 6 \;\Rightarrow\; Q_{s_{ref}} = -50000 \text{ VAR} \\ 6 \le t \le 8 \;\Rightarrow\; Q_{s_{ref}} = 0 \text{ VAR} \end{cases}$$

From Fig.16-17, it is shown that the active and reactive powers follow exactly their corresponding references with both controllers.

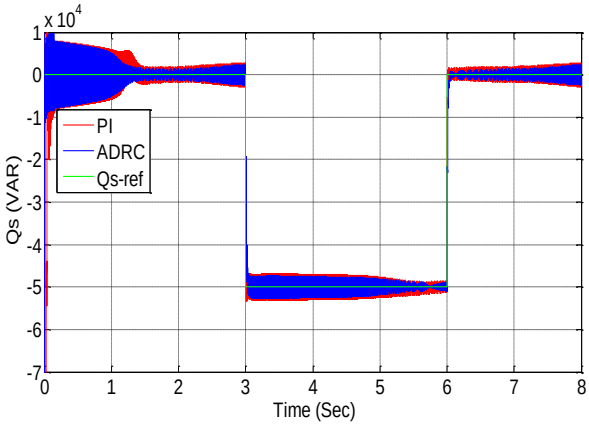

Fig. 16. Stator reactive power

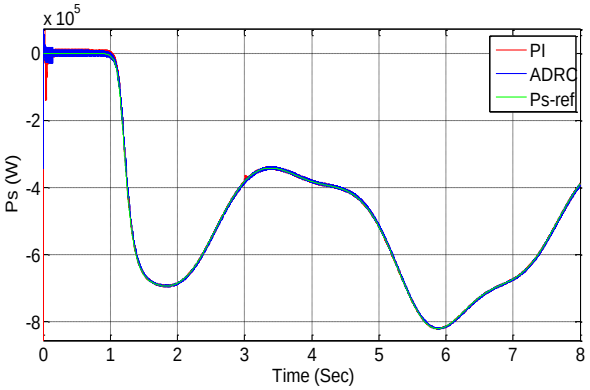

Fig. 17. Stator active power

The rotor currents i_{rd} and i_{rd} presented in Fig.18-19 vary exactly as their references deduced from the reactive power and the active power.

We notice from Fig.19 that the control using ADRC present a faster time response than the PI controller.

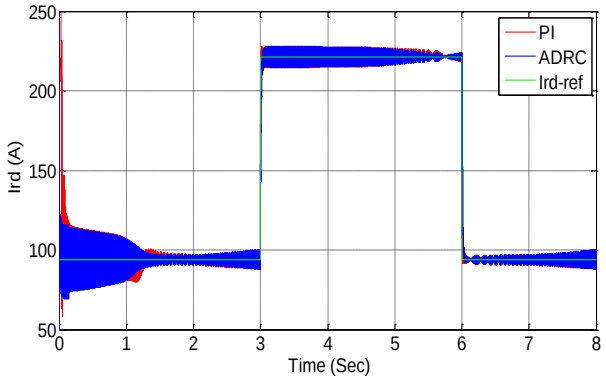

Fig. 18. Rotor current ird and its reference

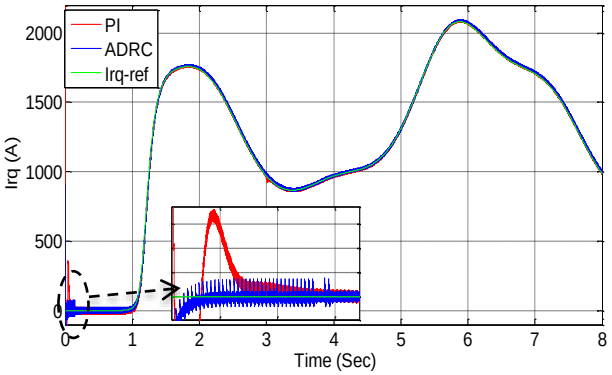

Fig. 19. Rotor current irq and its reference

The Fig. 20 and 21 show that the stator and rotor currents increase as wind speed increases.

The rotor and stator currents obtained by the DFIG are of three-phase and sinusoidal form, which shows a clean quality of energy produced without harmonics.

The following expression shows the frequency variation of the rotor currents with the variation of the slip, without taking into consideration, the start-up phase of the wind turbine:

$$\begin{cases} 0.006 \leq g \leq 0.257 \\ 0.3 \leq fr \leq 12.85 \text{ Hz} \end{cases}$$

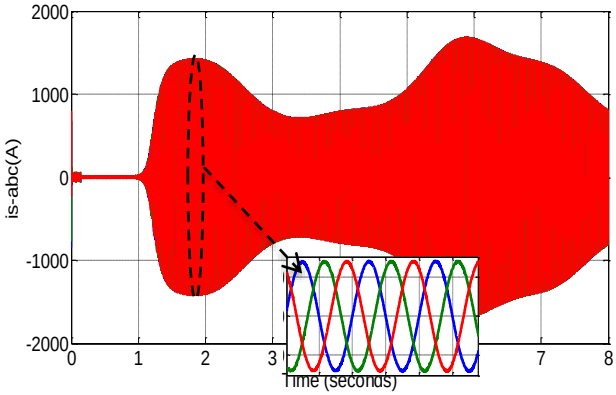

Fig. 20. The stator currents

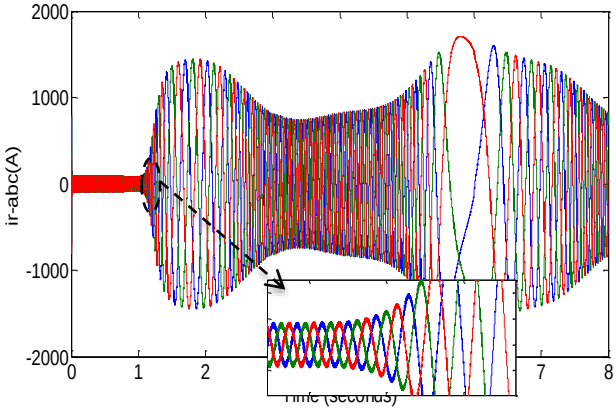

Fig. 21. The Rotor currents

5.2 Robustness:

The parameters of the regulators are dimensioned depending to the parameters of the machine model, which are assumed unchanged and fixed, but in reality, the systems are uncertain by presenting variations in their mathematical model.

To examine the performance of regulators a robustness test is established by varying the internal parameters of the machine model, as the rotor resistance Rr and the value of the rotor inductance which are the most stressed and deduce which one of the both controllers (PI & ADRC) is the most robust.

The control using PI regulator present an increase in response time and little oscillations compared to ADRC control strategy that has good robustness against parametric variations as noticed from Fig.22- 23.

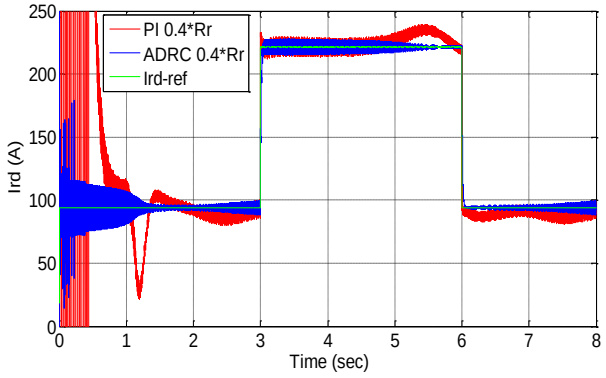

Fig. 22. Rotor current ird for 0.4*Rr and its reference

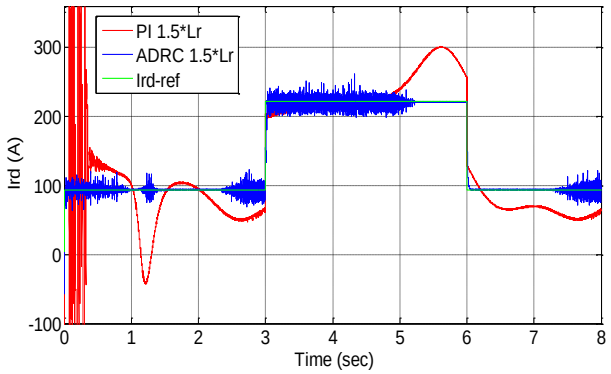

Fig. 23. Rotor current ird for 1.5*Lr and its reference

6. Conclusion

This work has been the opportunity to gather knowledge about doubly fed induction generator driven by the wind turbine.

The first section recalls the fundamental concepts of the WECS based on the double fed induction machine driven by its rotor-side converter, using the MPPT technique to maximize the power extracted from the wind.

To improve the quality of control two techniques are envisaged and compared in terms of robustness. A proportional-integral regulator that served as comparison reference, a new ADRC control strategy based on an extended state observer.

The purpose of these controllers is to control the active and reactive power exchange between the stator of the machine and the network by providing adequate rotor voltages.

Under the simulation results, we can deduce that the ADRC controller works efficiently when it comes to sensitivity to disturbances and strong robustness against the parametric variations of the DFIG than the control using a PI regulator that presents less good transient performance and more responses that are undesirable.

Appendix

Table 1. Parameters of turbine-generator

System	parameters	values
PARAMETERS OF THE TURBINE	Density of Air ρ Blade radius R Speed-up gear ratio, G Moment of inertia Power Coefficient Optimal relative wind speed Damping coefficient fv	1.225 kg/m^3 39m 90 J=10 kg.m² Cpmax=0.48 λ_{opt}=8.1 0.0024
PARAMETERS OF THE DFIG	Rated power Pn N°. of poles P Rated stator voltage Vs Nominal frequency f Stator inductance Ls Mutual inductance Lm Rotor resistance Rr Rotor inductance Lr	1.5 MW 2 400 V 50 Hz 0.0137 H 0.0135 H 0.021 0.0137 H
PI and ADRC Controllers	Kp Ki Rotor currents controller gain(ADRC) Kp-r Observation parameters l_1 l_2	0.1007 5.3278 130 1680 705600

References

[1] le Jury, D., BOUZEKRI, M. H., & ABDESSEMED, M. R. Production décentralisée de l'énergie électrique: Modélisation et contrôle d'une génératrice asynchrone auto excitée. (Standards and Reports)

[2] Poitiers, F. (2003). Etude et commande de génératrices asynchrones pour l'utilisation de l'énergie éolienne-machine asynchrone a cage autonome-machine asynchrone a double alimentation reliée au réseau (Doctoral dissertation, Université de Nantes).FAIROUZ, Kendouli. Centrale eolienne et qualite de l'energie electrique. 2017. (Standards and Reports)

[3] DOLATABADI, Soheil et TOHIDI, Sajjad. A Review on Position Sensorless Methods for Wind Generators. International Journal of Renewable Energy Research (IJRER), 2017, vol. 7, no 2, p. 476-488. (Article)

[4] FAIROUZ, Kendouli. Centrale eolienne et qualite de l'energie electrique. 2017. (Standards and Reports)

[5] BELFEDAL, Cheikh, ALLAOUI, Tayeb, BELABBAS, Belkacem, et al. Speed-Sensorless DFIG Wind Turbine for Power Optimization Using Fuzzy Sliding Mode Observer. International Journal of Renewable Energy Research (IJRER), 2017, vol. 7, no 2, p. 613-621. (Article)

[6] PUTRI, Adinda Ihsani, AHN, Minho, et CHOI, Jaeho. Speed sensorless fuzzy MPPT control of grid-connected PMSG for wind power generation. In : Renewable Energy Research and Applications (ICRERA), 2012

International Conference on. IEEE, 2012. p. 1-6. (Conference Paper)

[7] NAK, Handan et ERGENC, Ali Fuat. A new controller for variable speed wind turbine generator. In : Renewable Energy Research and Applications (ICRERA), 2013 International Conference on. IEEE, 2013. p. 446-451. (Conference Paper)

[8] Boukhriss, A., Essadki, A., Bouallouch, A., & Nasser, T. (2014, November). Maximization of generated power from wind energy conversion systems using a doubly fed induction generator with active disturbance rejection control. InComplex Systems (WCCS), 2014 Second World Conference on (pp. 330-335). IEEE. (Conference Paper)

[9] Chakib, R., Essadki, A., & Cherkaoui, M. (2014). Active Disturbance Rejection Control for Wind System Based On a DFIG. World Academy of Science, Engineering and Technology, International Journal of Electrical, Computer, Energetic, Electronic and Communication Engineering, 8(8), 1306-1315. (Article)

[10] AL-QUTEIMAT, Alaa, ROCCAFORTE, Alessandro, et SCHÄFER, Uwe. Performance improvement of direct torque control for doubly fed induction generator with 12 sector methodology. In : Renewable Energy Research and Applications (ICRERA), 2016 IEEE International Conference on. IEEE, 2016. p. 242-246. (Conference Paper)

[11] AYDIN, E., POLAT, A., et ERGENE, L. T. Vector control of DFIG in wind power applications. In : Renewable Energy Research and Applications (ICRERA), 2016 IEEE International Conference on. IEEE, 2016. p. 478-483. (Conference Paper)

[12] BOUZEKRI, Amina, ALLAOUI, Tayeb, DENAI, Mouloud, et al. Artificial Intelligence-Based Fault Tolerant Control Strategy in Wind Turbine Systems. INTERNATIONAL JOURNAL OF RENEWABLE ENERGY RESEARCH, 2017, vol. 7, no 2, p. 652-659. (Article)

[13] El Aimani, S., François, B., Minne, F., & Robyns, B. (2003, September). Modeling and simulation of doubly fed induction generators for variable speed wind turbines integrated in a distribution network. In 10th European conference on power electronics and applications, Toulouse, France. (Conference Paper)

[14] SARMA, Nur, APSLEY, Judith M., et DJUROVIC, Sinisa. Implementation of a conventional DFIG stator flux oriented control scheme using industrial converters. In : Renewable Energy Research and Applications (ICRERA), 2016 IEEE International Conference on. IEEE, 2016. p. 236-241. (Conference Paper)

[15] Benkahla, M., Taleb, R., & Boudjema, Z. (2016). Comparative Study of Robust Control Strategies for a Dfig-Based Wind Turbine. INTERNATIONAL JOURNAL OF ADVANCED COMPUTER SCIENCE AND APPLICATIONS, 7(2), 455-462. (Article)

[16] Bekakra, Y., & Attous, D. B. (2011). Sliding mode controls of active and reactive power of a DFIG with MPPT for variable speed wind energy conversion. Australian Journal of Basic and Applied Sciences, 5(12), 2274-2286. (Article)

[17] Boukhriss, A., Nasser, T., & Essadki, A. (2013). A linear active disturbance rejection control applied for dfig based wind energy conversion system.International Journal of Computer Science Issues (IJCSI), 10(2), 391-399. (Article)

[18] Herbst, G. (2013). A simulative study on active disturbance rejection control (ADRC) as a control tool for practitioners. Electronics, 2(3), 246-279. (Article)

[19] Zheng, Q. (2009). On active disturbance rejection control: stability analysis and applications in disturbance decoupling control (Doctoral dissertation, Cleveland State University). (Standards and Reports)

[20] Ghennam, T. (2011). Supervision d'une ferme éolienne pour son intégration dans la gestion d'un réseau électrique, Apports des convertisseurs multi niveaux au réglage des éoliennes à base de machine asynchrone à double alimentation (Doctoral dissertation, Ecole Centrale de Lille; Ecole Militaire polytechnique Alger). (Standards and Reports)